IEEE Access
Multidisciplinary | Rapid Review | Open Access Journal

Received March 8, 2021, accepted March 21, 2021, date of publication March 24, 2021, date of current version June 3, 2021.

Digital Object Identifier 10.1109/ACCESS.2021.3068412

Wideband Low RCS Antenna Based on Hybrid Absorptive-Diffusive Frequency Selective Reflector

BINCHAO ZHANG[1], LIANG LI[1], CHENG JIN[1], (Senior Member, IEEE), QIHAO LV[1], AND RAJ MITTRA[2,3], (Life Fellow, IEEE)

[1]School of Information and Electronics, Beijing Institute of Technology, Beijing 100081, China
[2]Electromagnetic Communication Laboratory, University of Central Florida, Orlando, FL 32816, USA
[3]Department of Electrical and Computer Engineering, King Abdulaziz University, Jeddah 21589, Saudi Arabia

Corresponding author: Liang Li (sparkle_ll@126.com)

This work was supported in part by the National Natural Science Foundation of China (NSFC) under Grant 61871036, and in part by the Open Project of the State Key Laboratory of Millimeter Waves under Grant K202018.

ABSTRACT A method for designing a wideband low radar cross section (RCS) antenna is proposed based on hybrid absorptive and diffusive frequency selective reflector (AD-FSR) in this paper. The low RCS antenna exhibits manifold frequency responses in three artificial bands, which are created by its different components. A simple U-slot patch antenna is borrowed, which is integrated with the diffusion metasurface, and placed under the absorptive sheet with about quarter wavelength. Then, the out-of-band incident wave is captured by the absorber in the lower frequency band, and diffused by the metasurface in the upper frequency band achieving the RCS reduction. The design strategies are explained and verified with the aid of the corresponding equivalent circuit model and current distributions. To illustrate the efficacy of the proposed approach, the low RCS antenna using the proposed hybrid AD-FSR structure is fabricated and tested, and the results demonstrate that the proposed structure is an attractive candidate for designing wideband low RCS antennas.

INDEX TERMS Absorber, diffusion metasurface, frequency selective surface, patch antenna, radar cross section (RCS).

I. INTRODUCTION

Low-observable designs play an important role in modern radar systems, while communication and radar antennas are often the culprits that contribute significantly to the radar signature of the target. Usually, antennas and antenna arrays are placed on a large metallic ground plate such as the vehicle-mounted and carrier-borne platforms, where the radar cross section (RCS) of the overall platform is mainly caused by the large ground plate. Hence, reducing the RCS of the large ground plate becomes a priority issue when designing these systems. At the same time, an eletromagnetci window should be open for various antennas or antenna arrays on the platform to transmit/receive electromagnetic wave. Traditional RCS reduction methods including integrated with metasurfaces or frequency selective surfaces (FSSs) based on the principle of phase cancellation [1]–[3], using wideband microwave absorber [4]–[6], or combining absorptive and diffusive structures [7], [8]. However, these techniques typically affect the performance of the antenna in an adverse way by reducing its gain and/or by distorting its radiation pattern in an undesirable manner. This has prompted the need to develop techniques for RCS reduction without degrading the performance of the antenna, and to do so over a wide frequency band.

Recently, a number of techniques have been proposed for reducing the RCS of an antenna without sacrificing its performance. Examples include replacing the ground plane of the antenna by an absorptive frequency selective service reflector (AFSR) [9]–[12]. The reflection band of the AFSR is designed to overlap with the operating band of antenna to maintain its performance, while absorbing the out-of-band waves impinging upon the antenna. Yet another method is to cover the antenna with an absorptive frequency selective

The associate editor coordinating the review of this manuscript and approving it for publication was Tutku Karacolak.

transmitter (AFST), which can be viewed as an absorptive radome [13]–[19]. The electromagnetic (EM) wave can pass through the AFST relatively unaffected in the passband, which works as the transmission window for the low RCS antenna, while the out-of-band incident wave is absorbed by the AFST. Unfortunately, most of these structures have only been applied to narrow band antennas or by bulking absorbing material. Furthermore, their RCS reduction bandwidth is relatively narrow, which is undesirable for many practical applications.

In order to extend the bandwidth of the RCS reduction band, structures with absorption and diffusion properties are hybridized and then integrated with the antenna [20]–[22]. The novel frequency-selective rasorbers are presented in [20], [21], which provide a high-efficiency transmission band with wide absorption and diffusion bands located at two sidebands. In addition, a slot array antenna is integrated with a hybrid metasurface for wideband monostatic and bistatic RCS reduction, which consists of an anisotropic frequency-selective absorber and a polarization rotation reflective surface [22].

In this paper, we present a methodology of designing low-RCS wideband antennas based on a proposed hybrid absorptive-diffusive frequency selective reflector (AD-FSR). The whole low RCS antenna we consider herein is a simple wideband U-slot patch antenna as an example, which is surrounded by a diffusion metasurface with an absorptive sheet placed above them. The diffusion metasurface shares the same ground plane of the patch antenna, and it scatters the field antiphase to the incident wave to reduce the RCS in the upper frequency band of the antenna. In addition, the metasurface works as a normal ground plate for the absorber without antiphase reflection in the lower frequency band, and then the absorptive sheet performs wideband absorptive characteristic together with the ground generated by the metasurface in the lower frequency band.

On the other hand, the absorptive sheet is penetrable in the working band of the antenna and the diffusion metasurface. Then, a window with a wide frequency band transparent to EM wave is realized in the middle operating band of the U-slot antenna, and two wide low RCS bands are achieved in both sides of the antenna's operating band. The design strategy is explained as well as verified with the aid of equivalent circuit model and the current distributions on the antenna. Finally, the studied antenna is fabricated and measured, and the measured results are in good agreement with the simulated ones which demonstrate the validation of the design procedure.

II. OPERATING PRINCIPLE

The key step involved in the design process of the wideband low RCS antenna is to construct two RCS reduction bands in the lower and upper sides of the antenna's operating band while maintaining a wide transparent window in the mid-band. In order to realize wideband RCS reduction performance, a wideband absorber working in the lower frequency band and a wideband diffusion metasurface designed to reduce the RCS in the upper frequency band are integrated together as shown in Fig. 1. Then, the whole structure consists of two layers separated by an air cavity, where the antenna is placed in the bottom layer and is surrounded by the diffusive metasurface while the absorber is placed above. It should be pointed out that a transparent window to EM wave with bandwidth controllable easily can be obtained painlessly just by tuning the two relative separate structures, and then the window can be used for various planar antennas, such as a wideband U-slot antenna used herein.

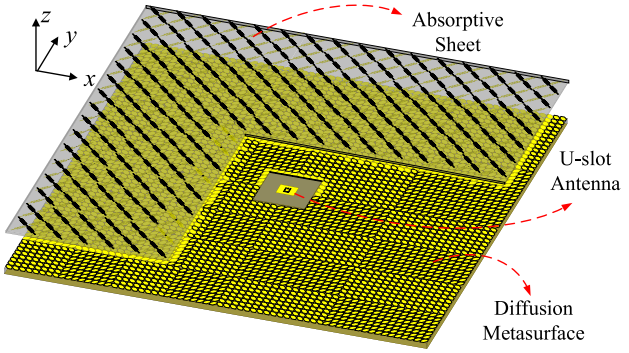

FIGURE 1. Configuration of the proposed low RCS antenna based on the hybrid AD-FSR.

The obtained low RCS antenna exhibits manifold frequency responses in different frequency bands, and the functionalities of its different components are also various, which is described in Fig. 2. Then, it requires that each component of the integrated structure works completely in cooperation with each other and creates three artificial bands with entirely different frequency responses.

As shown in Fig. 2, the upper layer of the proposed low RCS antenna is an absorptive sheet, and it works as a wideband absorber together with the ground plane created by the underneath diffusion metasurface layer. The absorber with the generated ground plane absorbs the incident wave in the lower frequency band around f_L, as shown in Fig. 2(a), while the upper absorptive sheet must be able to transmit the incident wave losslessly and then the wave be manipulated by the antenna or diffusion metasurface in the operating bands around f_M and f_H, as shown in Fig. 2(b) and (c). Hence, the absorber has two functionalities including absorptive frequency responses in the lower frequency band and transmitted frequency responses in the middle and upper frequency bands.

On the other hand, the diffusion metasurface surrounding the U-slot patch antenna should also have two functionalities, that it scatters the incident wave in the upper frequency band around f_H, as shown in Fig. 2(c), and it works as a normal ground plate without antiphase reflection response in the lower and middle frequency bands, as shown in Fig. 2(a) and (b). Finally, A transparent window is realized in the mid-frequency band around f_M, ensuring that the

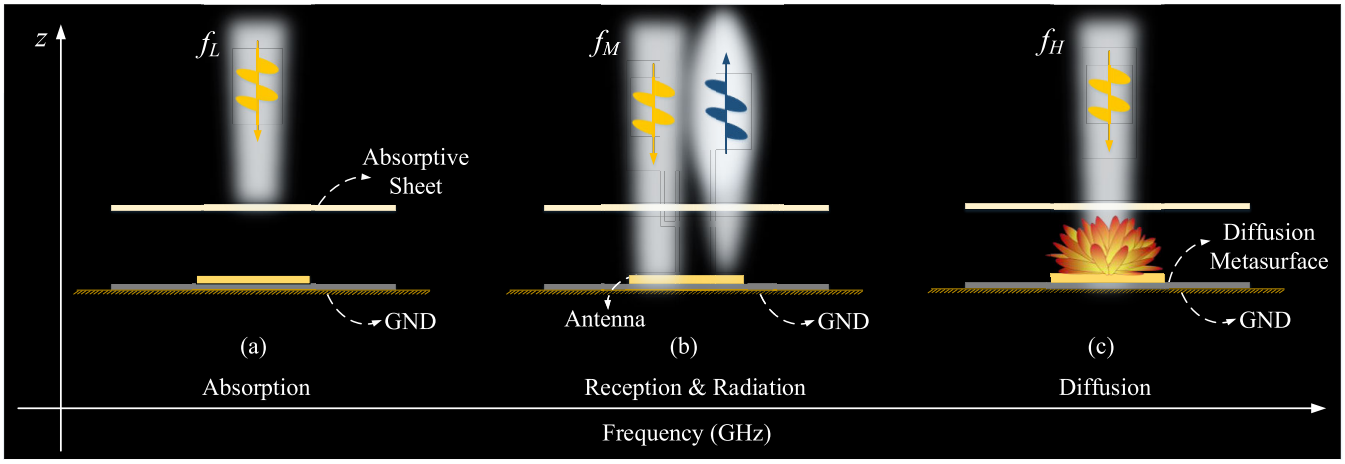

FIGURE 2. The different features of the proposed low-RCS antenna in (a) the lower frequency band f_L, (b) the middle frequency band f_M and (c) the upper frequency band f_H.

inserted antenna performance is not compromised either in the receive or the transmit mode, as shown in Fig. 2(b).

III. DESIGN OF HYBRID AD-FSR

A. WIDEBAND ABSORBER

The first step is to build the aforementioned absorber with wide RCS reduction band, and with transparent property in the higher frequency band when its ground plane is taken away. Fig. 3 illustrates the configuration of the designed wideband absorber and its geometries. The absorber is comprised of two miniaturized cross-strips embedded with chip-resistors in the center that are printed on the both sides of a thin substrate, whose thickness and relative permittivity are t_a and ε_r of 2.2, respectively. The period of the unit cell is p_a, and the lossy layer is placed at a distance of h_a above the conducting plate, which is approximately a quarter-wavelength at the center frequency of the absorption band. The cross-strips are miniaturized by using a meander line to improve the angular stability of the proposed absorber, as shown in Fig. 3(b).

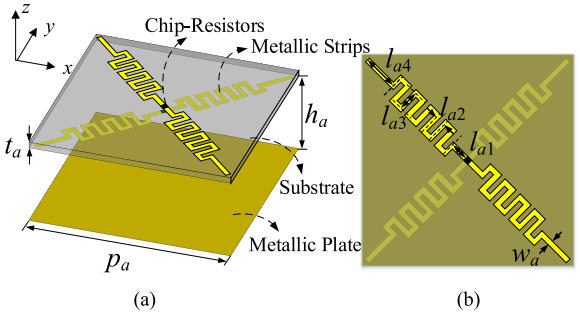

FIGURE 3. Configuration and geometries of the wideband absorber. (a) Perspective view. (b) Top view. (Physical dimensions: $p_a = 20$, $h_a = 15$, $t_a = 0.5$, $w_a = 0.5$, $l_{a1} = 2$, $l_{a2} = 1$, $l_{a3} = 2$, $l_{a4} = 3.5$. All dimensions are in millimeter).

Fig. 4 shows the simulated reflection and transmission characteristics of the proposed absorber derived by using the commercial solver HFSS. Master and Slave boundary conditions are used to represent the periodic boundary conditions of the unit cell and Floquet ports are used as the excitation ports. We observe from Fig. 4(a) that there are two resonances f_{a1} and f_{a2} within the absorber's operating frequency band at 3.41 GHz and 6.78 GHz, respectively, with the help of the ground plate, and the fractional bandwidth with reflectivity less than -10 dB is 96.2%. While an excellent transmission characteristic is realized from 8 to 20 GHz for the absorptive sheet only without the ground plate, as shown in Fig. 4(b), which can be utilized as the operating band for the antenna and diffusion metasurface as we predicted.

In order to gain insight into the existence of these two resonances and explain the absorption mechanism, an equivalent circuit model (ECM) of the absorber is established as the inset figure shown in Fig. 4(a). The miniaturized metallic strips printed on the substrate can be equivalently represented by a series *LC* circuit [23], and the absorber can be represented by an *RLC* circuit with a short-circuited transmission line of length h_a, which represents the conductor-backed air spacer. Then, the input surface admittance Y_{in} of the absorber is the sum of the admittance of the absorptive sheet Y_L and the air space Y_{sub}, which can be expressed as

$$Y_L = \frac{1}{R + j\left(\omega L_1 + \frac{1}{\omega C_1}\right)} = G_L + jB_L, \tag{1}$$

$$Y_{sub} = -jY_0 \cot \beta h_a = jB_{sub}, \tag{2}$$

where G_L and B_L are the conductance and susceptance components. They can be written as

$$G_L = \frac{\omega^2 RC^2}{\left(1 - \omega^2 LC^2\right)^2 + \omega^2 R^2 C^2}, \tag{3}$$

$$B_L = \frac{\omega C - \omega^3 LC^2}{\left(1 - \omega^2 LC^2\right)^2 + \omega^2 R^2 C^2}. \tag{4}$$

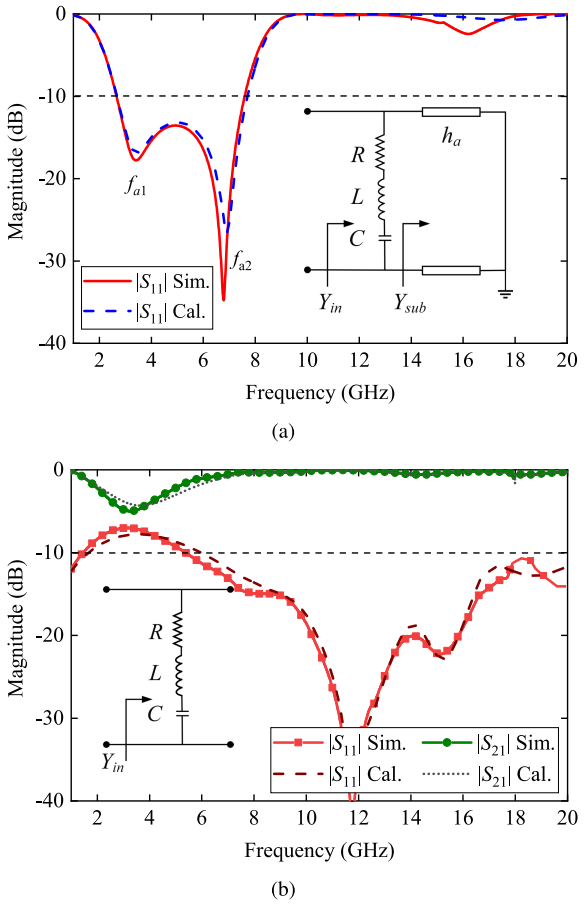

FIGURE 4. Desired S-parameters of absorber (a) with and (b) without the ground plate.

Then, we can obtain the reflection coefficient Γ as follows by using this equivalent circuit model [24]

$$\Gamma = \frac{Y_0 - Y_{in}}{Y_0 + Y_{in}} = \frac{(Y_0 - G_L) - j(B_L + B_{sub})}{(Y_0 + G_L) + j(B_L + B_{sub})}, \tag{5}$$

where Y_0 stands for the characteristic admittance of free space.

It is well known that the resonances can be produced when the imaginary part of the input admittance equals to zero [25], that is

$$B_L + B_{sub} = 0. \tag{6}$$

From 6, it is evident that there are two situations which can lead to resonance. The first of these occur when $B_L = B_{sub} = 0$, i.e., when both susceptance values are zero, which corresponding to the first resonance at frequency f_{a1}, while the second residence occurs when $B_L = -B_{sub} \neq 0$, i.e., when the susceptance of the strip exactly cancels the susceptance of the short-circuited transmission line, which corresponding to the second resonance at frequency f_{a2}. While for the absorptive sheet only without the ground plane, the equivalent circuit model is given in the inset figure of Fig. 4(b). At this case, the input surface admittance Y_{in} equals to Y_L, and the absorber only has one resonance at frequency f_{a1} when $B_L = 0$.

The equivalent inductances and capacitances for the metallic strip under the normal incidence can be evaluated by using the formulas given in [26]–[28], and the value of chip-resistor is determined for optimal frequency response. Then, the circuit model is conducted by using the following values: $R = 250\ \Omega$, $L = 17.9$ nH, $C = 0.056$ pF. The calculated frequency responses of the proposed absorber derived by using the circuit model are also shown in Fig. 4, which have seemed to be in good agreement with simulated results.

B. WIDEBAND POLARIZATION ROTATOR

Next, a wideband polarization rotator by using a two-dimensional periodic array of truncated square patches is designed, which can be utilized to construct the diffusion metasurface to reduce the antenna's RCS in the upper frequency band. Fig. 5 illustrates the configuration of the unit cell, and a truncated square patch is printed on the same dielectric substrate with the absorptive layer whereas its thickness is t_r. The topology follows the same period p_r along both the x- and y-directions, which is a quarter of the absorber's period. In addition, the dimensions of the long and short axes of the truncated square patch are l_{r1} and l_{r2}, respectively. The simulated cross- and co-reflection coefficients of the proposed rotator are shown in Fig. 6(a), which are represented by S_{12}^{yx} and S_{11}^{xx}, respectively. We see that a good polarization rotation performance is realized from 14.19 to 19.39 GHz, and the relative bandwidth is 31%. We also note that two resonances f_{r1} and f_{r2} are generated in the operating band at 15.25 GHz and 17.71 GHz, respectively.

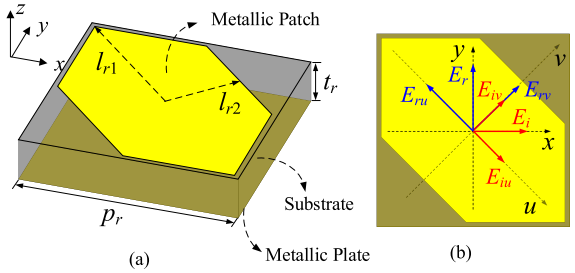

FIGURE 5. Configuration of the proposed wideband polarization rotator. (a) Perspective view. (b) Top view. (Physical dimensions: $p_r = 5$, $t_r = 1$, $l_{r1} = 3.25$, $l_{r2} = 1.75$. All dimensions are in millimeter).

In order to analyze the structural anisotropy and the underlying polarization mechanism, the incident wave along the x-axis is decomposed into two orthogonal components along the u- and v-axes, as shown in Fig. 5(b), which can be re-expressed as

$$\vec{E}_i = \frac{\sqrt{2}}{2}|E_0|(\hat{e}_u + \hat{e}_v), \tag{7}$$

where $\hat{e}_u$ and $\hat{e}_v$ are the unit vector along the u- and v-axes, respectively, and $|E_0|$ is the magnitude of the incident electric field. Then, we turn to the wave $\vec{E}_r$ reflected from the

polarization rotating surface, and it can also be represented as a sum of two orthogonal components

$$\vec{E}_r = \frac{\sqrt{2}}{2}|E_0|(\hat{e}_u|r_u|e^{j\varphi_u} + \hat{e}_v|r_v|e^{j\varphi_v}), \tag{8}$$

where $|r_u|$ and φ_u, as well as $|r_v|$ and φ_v are the corresponding magnitudes and shifted phases along the u- and v-axes, respectively. It should be mentioned that both the reflection magnitudes are unity ($|r_u| = |r_v| = 1$) owing to the presence of the PEC ground plane at the bottom.

Because the x-polarized wave has both the components along the u- and v-axes, the resonances along the long and short axes of the truncated square patch will be excited simultaneously under a x-polarized incidence. The phase difference of the u-oriented and v-oriented reflected waves ($\Delta\varphi = \varphi_u - \varphi_v$) is plotted in Fig. 6(b), and we observe that the phase difference is different in and out of the operating band. The in-band phase difference $\Delta\varphi$ is approximately 180° with a tolerance less than 30°, which results in a good polarization rotation performance according to (7) and (8) [29]. On the other hand, the phase difference is almost zero in the out-of-band, which means that the rotator can be viewed as a normal ground plane at the outer band frequencies.

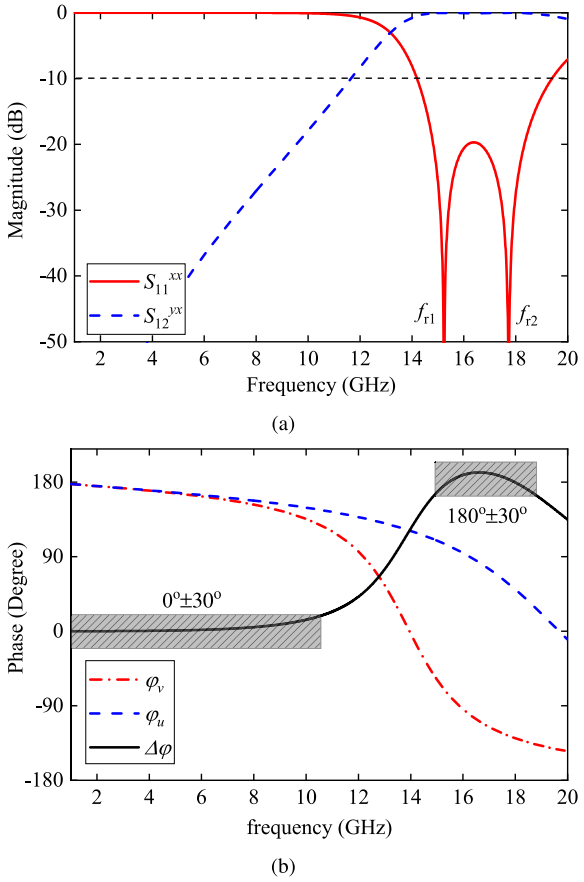

FIGURE 6. Simulated results of the proposed polarization rotator. (a) The magnitude of reflection coefficients. (b) The phase of reflection coefficients for *u*- and *v*-polarized reflected waves.

In order to further explain the physical mechanism of the proposed polarization rotator, the simulated current distributions on the top truncated square patch and the bottom ground plate at the resonant frequencies f_{r1} and f_{r2} are shown in Fig. 7. The lower resonance at f_{r1} is excited along the long axis of the truncated square patch, while the upper resonance at f_{r2} is excited along the short axis. In addition, the currents flowing through the metallic patch are anti-parallel to those on the ground plate for both two resonances. Hence the current loops are formed in the intermediate dielectric layer, and this resonance is known as magnetic resonance [30].

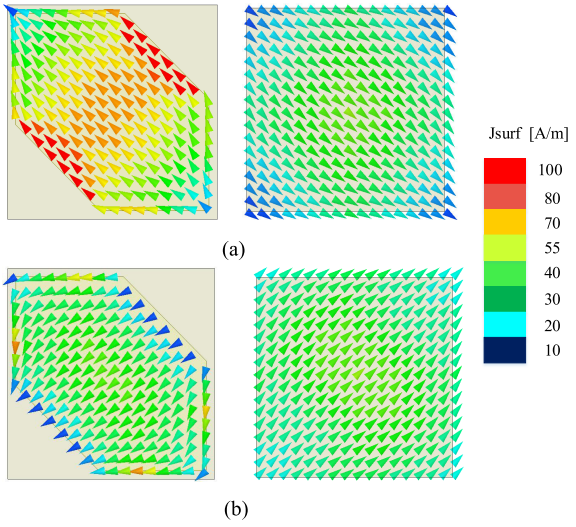

FIGURE 7. Simulated current distributions on the top truncated square patch and bottom ground plate at resonant frequencies (a) f_{r1} and (b) f_{r2}.

C. HYBRID ABSORPTIVE-DIFFUSIVE FREQUENCY SELECTIVE REFLECTOR

The absorber and polarization rotator are integrated together realizing the proposed hybrid AD-FSR to obtain two wide RCS reduction bands on both above and below the operating mid-band frequency, while maintaining a transparent window in the mid-band. Fig. 8(a) shows the configuration of the unit cell of the obtained hybrid AD-FSR, while the absorptive sheet is placed above a 4 × 4 array of the polarization rotator and they share the same ground plate.

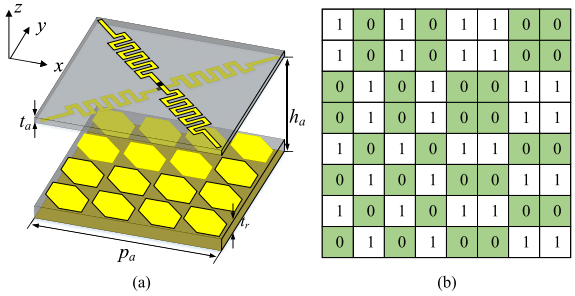

FIGURE 8. (a) Configuration of the proposed hybrid AD-FSR and (b) the element distributions of the diffusion metasurface.

Fig. 9 displays the simulated reflection coefficients of the hybrid AD-FSR arrayed in periodic pattern, and it is seen that a lower absorption band ranging from 2.59 to 7.67 GHz with two resonances at f'_{a1} (3.2 GHz) and f'_{a2} (7.1 GHz). Additionally, good polarization rotation performance is also achieved with two resonances at f'_{r1} (15.12 GHz) and f'_{r2} (17.58 GHz) in the upper frequency band ranging from 13.73 to 18.23 GHz, which is employed to reduce the RCS of the antenna by configuring it as the checkerboard metasurface or the diffusive metasurface. Compared with the independent absorber and polarization rotator, the widths of the lower and upper frequency bands are both slightly wider, which can be attributed to the mutual coupling between them.

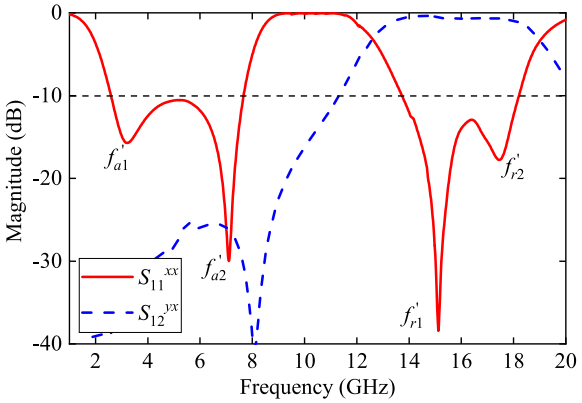

FIGURE 9. Simulated reflection coefficients of the combination of the absorber and the polarization rotator.

According to the array theory [31]–[33], when the incident wave illuminates on a metasurface with an array of $M \times N$, the scattering field can be described as

$$SP(\theta, \varphi) = \cos\theta \sum_{n=1,m=1}^{M,N} e^{-j(\frac{2\pi}{\lambda}\sin\theta)(\cos\varphi \cdot mP + \sin\varphi \cdot nP) + \varphi_{mn}}, \tag{9}$$

where θ and φ are the elevation and azimuth angles, respectively, (m, n) is the position of the element, and φ_{mn} is the scattering phase of each element. In order to meet the requirement of the phase cancellation principle, the metasurface consists of the proposed polarization rotator (Bit 0) and its antiphase counterpart (Bit 1), whose cross-polarized reflected waves share the same amplitude but opposite phases.

It should be pointed out that the '0' element is defined as the square block which includes 8×8 'Bit 0' unit cells with a 0 phase response, and the '1' element is defined as the square block comprising of 8×8 'Bit 1' unit cells with a π phase response, which is a trade-off between RCS reduction performance and processing costs. Then, a 10-dB RCS reduction can be realized according to

$$RCS_{reduction} = 10\lg|\frac{A_1 e^{j\varphi_1} + A_2 e^{j\varphi_2}}{2}|^2, \tag{10}$$

where A_1 and A_2, φ_1 and φ_2 are the corresponding reflection amplitudes and phases of 'Bit 0' and 'Bit 1', respectively.

For the sake of obtaining a good RCS reduction performance, the scattering pattern is manipulated by using the ergodic algorithm. The peak value of the scattering field can be expressed as the fitness function

$$fitness = \max(SP(\theta, \varphi)). \tag{11}$$

Then, the ergodic algorithm is employed in MATLAB to find a minimum value of fitness function at the direction of the normal incidence, and a good sequence of the diffusive metasurface contains 8×8 equal-sized square blocks is obtained, as shown in Fig. 8(b).

IV. DESIGN OF LOW-RCS ANTENNA

A simple U-slot patch antenna is borrowed here to demonstrate the proposed concept of the wideband low RCS antenna design based on the designed hybrid AD-FSR, whose geometries are shown in Fig. 10. Then, the simple U-slot patch antenna is integrated with the proposed hybrid AD-FSR structure to realize a low-RCS wideband antenna, as shown in Fig. 1. The designed U-slot antenna is inserted in the obtained diffusion metasurface above by replacing several truncated square patches, while the wideband absorptive sheet keeps unchanged as the same as the above design one.

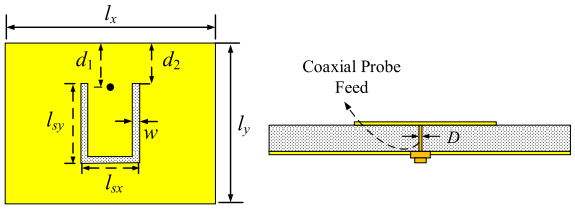

FIGURE 10. Configuration of conventional U-slot patch antenna. (Physical dimensions: $l_x = 12$, $l_y = 9$, $l_{sx} = 3.4$, $l_{sy} = 4.7$,$w = 0.4$, $d_1 = 2.5$, $d_2 = 2$, $D = 0.92$. All dimensions are in millimeter.)

The antenna operates in the frequency band ranging from 9.03 to 11 GHz, as shown in Fig. 11(a), which is simulated by using the HFSS simulations with radiation boundary condition. Compared with the U-slot patch antenna with same dimensions, the operating bandwidth of the present design of the low-RCS antenna is slightly wider, which is mainly attributable to the lower quality factor which is reduced by the introduction of the added absorber and diffusion metasurface. Fig. 11(b) and (c) show the simulated radiation patterns of the proposed and conventional antenna in *xoz* and *yoz* planes, respectively. It is seen that the simulated broadside gain of the designed low RCS antenna is approximately 7.40 dBi at 10 GHz, which is 0.66 dBi less than the conventional antenna without integrated with hybrid AD-FSR structure. It should be noted that the gain loss is mainly caused by the dielectric substrate of absorptive sheet. In addition, the antenna efficiency at 10 GHz is about 70.8%.

Next, to verify and validate the designed antenna with the low RCS characteristic, we compare its performance with that of the conventional U-slot patch antenna with PEC ground plane. Fig. 12(a) presents the monostatic RCS of the

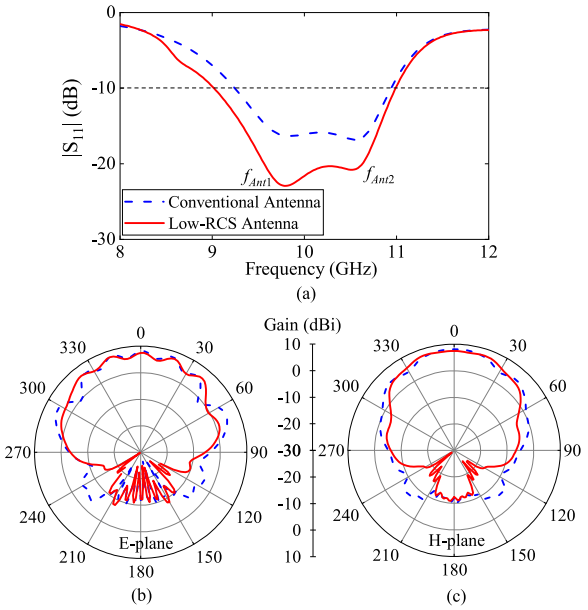

FIGURE 11. Simulated results of conventional and low-RCS U-slot patch antenna in radiation mode. (a) Reflection coefficients. Radiation pattern in (b) E-plane and (c) H-plane at 10 GHz.

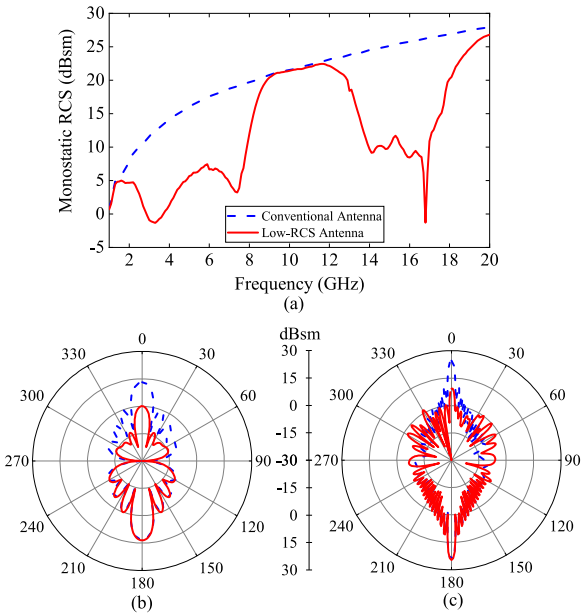

FIGURE 12. Simulated results of conventional and low-RCS U-slot patch antenna in scattering mode. (a) Monostatic RCS. (b) Bistatic scattering pattern at (b) 4 GHz in the absorption band and (c) 15 GHz in the diffusion band.

two antennas, and it confirms that RCS reduction is achieved over two wide frequency bands, both in the lower and upper frequency regimes, and without compromising the performance of the antenna in the mid-frequency range. In the lower frequency band, the incident wave from the $+z$-direction is absorbed as shown in Fig. 12(b), and on the other hand, it is diffused by the metasurface when the frequency of the incident wave is in the upper frequency band as shown in Fig. 12(c).

V. FABRICATION AND MEASUREMENT

To validate the radiation and RCS reduction performance of the proposed integrated hybrid AD-FSR U-slot patch antenna by measurements, we have fabricated a prototype of the designed antenna whose dimensions is 320 mm×320 mm as shown in Fig. 13. We note that 16 nylon screws whose lengths are 15 mm were used to attach the absorptive sheet to the metasurface layer. The upper layer shown in Fig. 13(a) is the absorptive sheet, and the two chip resistors with 0402 package (250 Ω) are soldered on the top and bottom sides of each unit cell. Fig. 13(b) shows the upper surface of the bottom substrate, containing the U-slot patch and the diffusion metasurface. The U-slot patch antenna is fed by a coaxial SMA connector. The absorber, as well as the patch antenna and diffusion metasurface are printed on a Rogers RT/duroid 5880 dielectric slab ($\varepsilon_r = 2.2$, $tan\delta = 0.0009$) using the PCB technology, with the thicknesses of 1 mm and 0.5 mm, respectively.

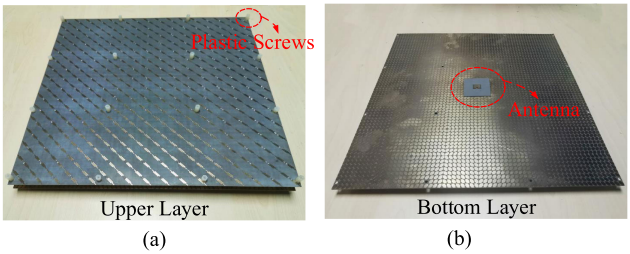

FIGURE 13. Photographs of the fabricated low-RCS antenna.

The test system for measuring the prototype is shown in Fig. 14, and two different types of systems are used to measure the RCS reduction and radiation performance of the designed antenna. When measuring the radiation pattern, the antenna is placed in a chamber and fed by the coaxial probe, as shown in Fig. 14(a). The measured reflection coefficient and radiation patterns of the fabricated antenna are shown in Fig. 15. The measured results show that the designed antenna works from 8.91 to 11.1 GHz, which is a little wider than the simulation results, and we conjecture it

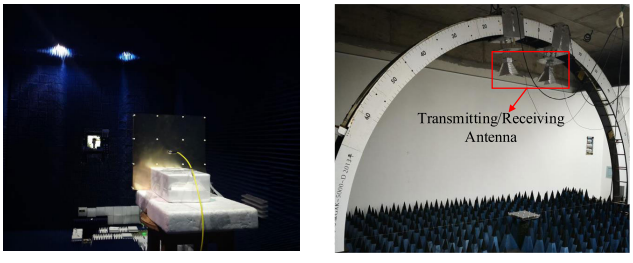

FIGURE 14. Test system for measurement of (a) radiation performance and (b) reflectivity in the chamber.

TABLE 1. Comparison With State-of-the-art Designs in the Literature.

Reference	Antenna type	Low RCS reduction bandwidth (%)	Antenna bandwidth (%)	Center frequency f_0 (GHz)	Upper RCS reduction bandwidth (%)
[9]	Dipole	26	11.5	8.7	16.7
[10]	Dipole	64.7	14.5	5.5	42.4
[13]	Patch	43.9	4	8.9	26.08
[14]	Patch	60.3	3	10	20.4
[34]	Patch	20.2	1	10	45.2
This work	Patch	90	21.9	10	27.6

is attributable to the fabrication tolerance and material loss. Fig. 15(b) and (c) show that the measured gain is only 0.3 dB lower than the simulated result because of losses in the SMA connector and the coaxial line, which is reasonable. Additionally, the cross-polarization of the antenna is low enough to indicate a good linear polarization radiation performance.

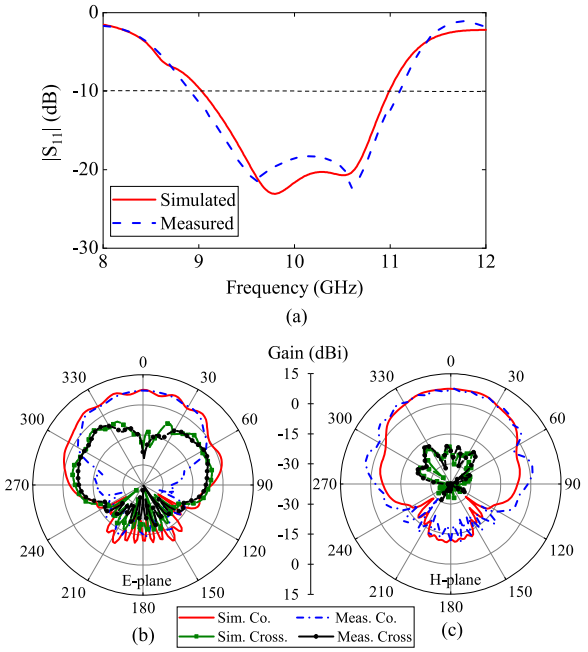

FIGURE 15. Simulated and measured results of the proposed antenna in radiation mode. (a) Reflection coefficients. Radiation pattern in (b) E-plane and (c) H-plane at 10 GHz.

The simulated and measured monostatic RCS reduction of the proposed antenna is shown in Fig. 16 for the normally and obliquely impinging plane waves. The measurement setup is shown in Fig. 14(b), and the measured results are seemed to agree well with the simulated ones. We note that the RCS reduction is obtained in the lower frequency band from 2.9 to 7.65 GHz, as well as in the upper frequency band from 13.6 to 17.95 GHz, with the fractional bandwidth of 90% and 27.6%, respectively, while it is almost negligible in the mid-frequency band, which is the operating band of the U-slot antenna. Additionally, we can observe that the RCS reduction performance in the lower frequency band is relatively stable

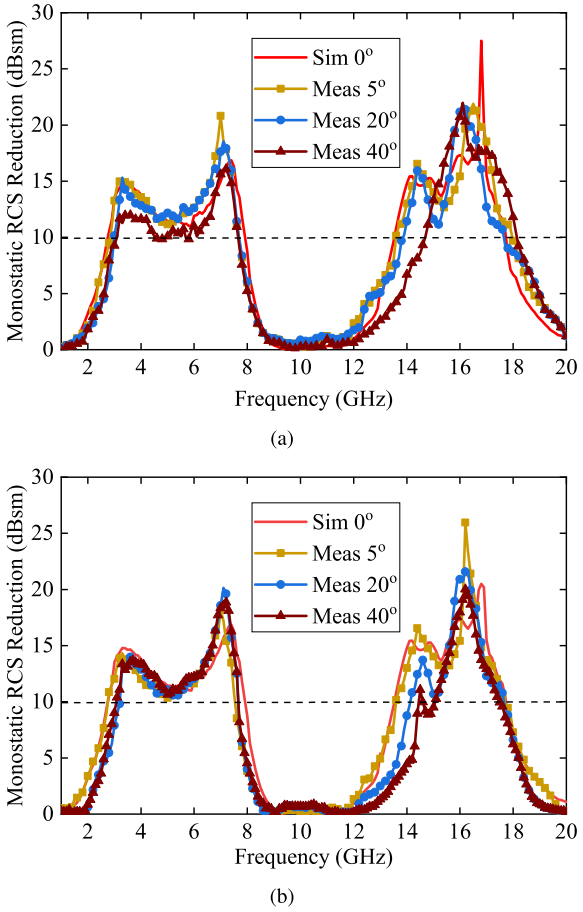

FIGURE 16. Simulated and measured monostatic RCS reduction of the proposed antenna under (a) TE-polarization and (b) TM-polarization for different incident angles.

with oblique incident wave, although the bandwidth in the upper frequency band becomes narrower when the incident angle increases to 40°.

In order to better understand the advantages of the designed low-RCS antenna, we have carried out a comparative study off the present antenna with other low-RCS antennas containing AFST and AFSR that have been reported elsewhere, and the results of the study are presented in Table 1. The table shows that in addition to realizing the wide operated band, the present antenna indeed realizes a lower RCS in

both the lower and upper bands shouldering the operating frequency band of the antenna, with little compromise the gain of the antenna in its operating band. The comparison presented in the above table clearly demonstrates that the hybrid AD-FSR is effective for wideband RCS reduction of large metallic platform while providing electromagnetic windows for various antennas or antenna arrays on the platform.

VI. CONCLUSION

In this paper, we have presented the design of a low-RCS wide-band antenna which incorporates a hybrid absorptive-diffusive frequency selective reflector with the antenna to reduce its RCS without compromising its radiation performance. The topology of the structure consisting well cooperative absorptive sheet, diffusion metasurface and antenna was discussed at first. Then, the absorptive structure is adopted by comprising miniaturized metallic cross-strips loaded with chip-resistors, and the diffusion metasurface is formed by a polarization rotator constructed by combining truncated square patches and their antiphase counterparts. An example of the designed antenna has been fabricated and measured, and the measured results demonstrate that the antenna achieves a wide operating band. Moreover, a wideband out-of-band RCS reduction is achieved for dual-polarized incidences.

REFERENCES

[1] Y. Liu, K. Li, Y. Jia, Y. Hao, S. Gong, and Y. J. Guo, "Wideband RCS reduction of a slot array antenna using polarization conversion metasurfaces," *IEEE Trans. Antennas Propag.*, vol. 64, no. 1, pp. 326–331, Jan. 2016.

[2] D. Sang, Q. Chen, L. Ding, M. Guo, and Y. Fu, "Design of checkerboard AMC structure for wideband RCS reduction," *IEEE Trans. Antennas Propag.*, vol. 67, no. 4, pp. 2604–2612, Apr. 2019.

[3] F. Yuan, H.-X. Xu, X.-Q. Jia, G.-M. Wang, and Y.-Q. Fu, "RCS reduction based on Concave/Convex-chessboard random parabolic-phased metasurface," *IEEE Trans. Antennas Propag.*, vol. 68, no. 3, pp. 2463–2468, Mar. 2020.

[4] T. Liu, X. Cao, J. Gao, Q. Zheng, W. Li, and H. Yang, "RCS reduction of waveguide slot antenna with metamaterial absorber," *IEEE Trans. Antennas Propag.*, vol. 61, no. 3, pp. 1479–1484, Mar. 2013.

[5] Y. Liu and X. Zhao, "Perfect absorber metamaterial for designing low-RCS patch antenna," *IEEE Antennas Wireless Propag. Lett.*, vol. 13, pp. 1473–1476, 2014.

[6] B. Zhang, C. Jin, and Z. Shen, "Low-profile broadband absorber based on multimode resistor-embedded metallic strips," *IEEE Trans. Microw. Theory Techn.*, vol. 68, no. 3, pp. 835–843, Mar. 2020.

[7] Y. Zhuang, G. Wang, J. Liang, and Q. Zhang, "Dual-band low-scattering metasurface based on combination of diffusion and absorption," *IEEE Antennas Wireless Propag. Lett.*, vol. 16, pp. 2606–2609, 2017.

[8] Y. Zhuang, G. Wang, Q. Zhang, and C. Zhou, "Low-scattering tri-band metasurface using combination of diffusion, absorption and cancellation," *IEEE Access*, vol. 6, pp. 17306–17312, 2018.

[9] P. Mei, X. Q. Lin, J. W. Yu, A. Boukarkar, P. C. Zhang, and Z. Q. Yang, "Development of a low radar cross section antenna with band-notched absorber," *IEEE Trans. Antennas Propag.*, vol. 66, no. 2, pp. 582–589, Feb. 2018.

[10] H. Huang, Z. Shen, and A. A. Omar, "3-D absorptive frequency selective reflector for antenna radar cross section reduction," *IEEE Trans. Antennas Propag.*, vol. 65, no. 11, pp. 5908–5917, Nov. 2017.

[11] B. Zhang, C. Jin, and Z. Shen, "Absorptive frequency-selective reflector based on bent metallic strip embedded with chip-resistor," *IEEE Trans. Antennas Propag.*, vol. 68, no. 7, pp. 5736–5741, Jul. 2020.

[12] B. Zhang, C. Jin, Q. Lv, J. Chen, and Y. Tang, "Low-RCS and wideband reflectarray antenna with high radiation efficiency," *IEEE Trans. Antennas Propag.*, early access, Dec. 21, 2020, doi: 10.1109/TAP.2020.3044660.

[13] P. Mei, X. Q. Lin, J. W. Yu, P. C. Zhang, and A. Boukarkar, "A low radar cross section and low profile antenna co-designed with absorbent frequency selective radome," *IEEE Trans. Antennas Propag.*, vol. 66, no. 1, pp. 409–413, Jan. 2018.

[14] Q. Chen, M. Guo, D. Sang, Z. Sun, and Y. Fu, "RCS reduction of patch array antenna using anisotropic resistive metasurface," *IEEE Antennas Wireless Propag. Lett.*, vol. 18, no. 6, pp. 1223–1227, Jun. 2019.

[15] Y. Han, L. Zhu, Y. Bo, W. Che, and B. Li, "Novel low-RCS circularly polarized antenna arrays via frequency-selective absorber," *IEEE Trans. Antennas Propag.*, vol. 68, no. 1, pp. 287–296, Jan. 2020.

[16] B. Zhang, C. Jin, K. Chen, and Z. Shen, "Aperture antenna embedded notched parallel plate waveguide and its application to dual-polarized 3-D absorptive frequency-selective transmission structure," *IEEE Access*, vol. 8, pp. 94833–94841, 2020.

[17] Q. Chen, S. Yang, J. Bai, and Y. Fu, "Design of absorptive/transmissive frequency-selective surface based on parallel resonance," *IEEE Trans. Antennas Propag.*, vol. 65, no. 9, pp. 4897–4902, Sep. 2017.

[18] M. Guo, Q. Chen, D. Sang, Y. Zheng, and Y. Fu, "Dual-polarized dual-band frequency selective rasorber with low insertion loss," *IEEE Antennas Wireless Propag. Lett.*, vol. 19, no. 1, pp. 148–152, Jan. 2020.

[19] M. Guo, Y. Zheng, Q. Chen, L. Ding, D. Sang, F. Yuan, T. Guo, and Y. Fu, "Analysis and design of a high-transmittance performance for varactor-tunable frequency selective surface," *IEEE Trans. Antennas Propag.*, early access, Dec. 23, 2020, doi: 10.1109/TAP.2020.3045517.

[20] L. Zhou and Z. Shen, "Hybrid frequency-selective rasorber with low-frequency diffusion and high-frequency absorption," *IEEE Trans. Antennas Propag.*, vol. 69, no. 3, pp. 1469–1476, Mar. 2021, doi: 10.1109/TAP.2020.3018537.

[21] Q. Lv, C. Jin, B. Zhang, and Z. Shen, "Hybrid absorptive-diffusive frequency selective radome," *IEEE Trans. Antennas Propag.*, early access, Nov. 18, 2020, doi: 10.1109/TAP.2020.3037644.

[22] Y. Liu, Y. Jia, W. Zhang, and F. Li, "Wideband RCS reduction of a slot array antenna using a hybrid metasurface," *IEEE Trans. Antennas Propag.*, vol. 68, no. 5, pp. 3644–3652, May 2020.

[23] J. S. Hong and M. J. Lancaster, *Microstrip Filter for RF/Microwave Ap plications*. New York, NY, USA: Wiley, 2001.

[24] D. M. Pozar, *Microwave Engineering*. New York, NY, USA: Wiley, 2005.

[25] Y. Shang, Z. Shen, and S. Xiao, "On the design of single-layer circuit analog absorber using double-square-loop array," *IEEE Trans. Antennas Propag.*, vol. 61, no. 12, pp. 6022–6029, Dec. 2013.

[26] R. J. Langley and E. A. Parker, "Double-square frequency-selective surfaces and their equivalent circuit," *Electron. Lett.*, vol. 19, no. 17, pp. 675–676, 1983.

[27] R. J. Langley and E. A. Parker, "Equivalent circuit model for arrays of square loops," *Electron. Lett.*, vol. 18, no. 7, pp. 294–296, Apr. 1982.

[28] Z. L. Wang, K. Hashimoto, N. Shinohara, and H. Matsumoto, "Frequency-selective surface for microwave power transmission," *IEEE Trans. Microw. Theory Techn.*, vol. 47, no. 10, pp. 2039–2042, Oct. 1999.

[29] M. K. T. Al-Nuaimi, W. Hong, and Y. He, "Design of diffusive modified chessboard metasurface," *IEEE Antennas Wireless Propag. Lett.*, vol. 18, no. 8, pp. 1621–1625, Aug. 2019.

[30] Q. Lv, C. Jin, B. Zhang, and Z. Shen, "Frequency-scanning multi-polarization antennas," *IEEE Trans. Antennas Propag.*, vol. 68, no. 11, pp. 7245–7254, Nov. 2020.

[31] C. A. Balanis, *Antenna Theory: Analysis and Design*, 4th ed. Hoboken, NJ, USA: Wiley, 2016.

[32] X. Liu, J. Gao, L. Xu, X. Cao, Y. Zhao, and S. Li, "A coding diffuse metasurface for RCS reduction," *IEEE Antennas Wireless Propag. Lett.*, vol. 16, pp. 724–727, 2017.

[33] Y. Pang, Y. Li, B. Qu, M. Yan, J. Wang, S. Qu, and Z. Xu, "Wideband RCS reduction metasurface with a transmission window," *IEEE Trans. Antennas Propag.*, vol. 68, no. 10, pp. 7079–7087, Oct. 2020.

[34] H. Jiang, Z. Xue, W. Li, W. Ren, and M. Gao, "Low-RCS high gain partially reflecting surface antenna with metamaterial ground plane," *IEEE Trans. Antennas Propag.*, vol. 64, no. 9, pp. 4127–4132, Sep. 2016.

BINCHAO ZHANG was born in Zhejiang, China, in 1992. He received the B.S. and M.S. degrees in electronic information engineering from the Nanjing University of Science and Technology (NJUST), Nanjing, China, in 2015 and 2018, respectively. He is currently pursuing the Ph.D. degree in electronic science and technology with the Beijing Institute of Technology (BIT), Beijing, China.

His research interests include microwave circuit analog absorber and frequency selected surface.

LIANG LI was born in Sichuan, China, in 1985. He received the B.S. and M.S. degrees in electromagnetic field and microwave technology from the University of Electronic Science and Technology of China (UESTC), Chendu, China, in 2007 and 2010, respectively. He is currently pursuing the Ph.D. degree in electronic science and technology with the Beijing Institute of Technology (BIT), Beijing, China.

His research interests include microwave circuit analog absorber and frequency selected surface.

CHENG JIN (Senior Member, IEEE) received the B.Eng. degree in electronic engineering from the University of Electronic Science and Technology of China (UESTC), Chengdu, China, in 2007, and the Ph.D. degree in communication engineering from Nanyang Technological University (NTU), Singapore, in 2012.

From 2011 to 2013, he was with the Institute of Microelectronics, Agency for Science, Technology and Research, Singapore. Since January 2014, he has been an Associate Professor with the School of Information and Electronics, Beijing Institute of Technology, Beijing, China. He has published and presented over 60 technical articles in journals/conferences. His current research interests include the design of microwave and millimeter-wave antennas, frequency selective surfaces and circuits, and microwave radar techniques.

Dr. Jin was a TPC Member of the 2014 IEEE Symposium on Wireless Technology and Applications (ISWTA 2014). He was a recipient of the 2011 ICICS Recognition of High Quality Paper Award, Singapore, and the 2012 IEEE Singapore MTT/AP Chapter Best Student Paper Contest Award. He has served on review boards for various technical journals, including the IEEE TRANSACTIONS ON ANTENNA AND PROPAGATION, the IEEE ANTENNAS AND WIRELESS PROPAGATION LETTERS, the IEEE TRANSACTIONS ON MICROWAVE THEORY AND TECHNIQUES, the IEEE MICROWAVE AND WIRELESS COMPONENTS LETTERS, and the *IET Electronics Letters*. He was a Designated Reviewer of the ISWTA 2013.

QIHAO LV was born in China, in 1994. He received the B.Eng. degree in communication engineering from the Nanjing University of Science and Technology (NJUST), Nanjing, China, in 2016. He is currently pursuing the Ph.D. degree in electronic science and technology with the Beijing Institute of Technology (BIT), Beijing, China.

His research interests include the design of microwave and millimeter-wave antennas and frequency-selective structures.

RAJ MITTRA (Life Fellow, IEEE) was a Professor with the Department of Electrical and Computer Engineering, University of Illinois at Urbana–Champaign, Champaign, IL, USA, from 1957 to 1996, and the Department of Electrical and Computer Engineering, Penn State University, State College, PA, USA, from 1996 to 2015. He is currently a Professor with the Department of Electrical Engineering and Computer Science Department, University of Central Florida, Orlando, FL, USA, where he is the Director of the Electromagnetic Communication Laboratory. He holds the position of a Hi-Ci professor with King Abdulaziz University, Jeddah, Saudi Arabia. He is also a Principal Scientist and a President of RM Associates.

Dr. Mittra was a recipient of the Guggenheim Fellowship Award, in 1965, the IEEE Centennial Medal, in 1984, the IEEE Millennium Medal, in 2000, the IEEE/AP-S Distinguished Achievement Award, in 2002, the Chen-To Tai Education Award, in 2004, the IEEE Electromagnetics Award, in 2006, and the IEEE James H. Mulligan Award, in 2011. He was a President of AP-S. He served as an Editor for the Transactions of the Antennas and Propagation Society. He is also serving as the Co-Editor-in-Chief for the e-Journal *FERMAT*.